ISSN 0023-1584, Kinetics and Catalysis, 2011, Vol. 52, No. 5, pp. 761–769. © Pleiades Publishing, Ltd., 2011.
Original Russian Text © O.B. Belskaya, N.N. Leont'eva, T.I. Gulyaeva, V.A. Drozdov, V.P. Doronin, V.I. Zaikovskii, V.A. Likholobov, 2011, published in Kinetika i Kataliz, 2011, Vol. 52, No. 5, pp. 778–786.

Formation of Platinum Sites on Layered Double Hydroxides Type Basic Supports: I. Effect of the Nature of the Interlayer Anion on the Structure Characteristics of the Layered Aluminum–Magnesium Hydroxide and the Formation of an Oxide Phase

O. B. Belskaya[a, b], N. N. Leont'eva[a], T. I. Gulyaeva[a], V. A. Drozdov[a, b], V. P. Doronin[a, b], V. I. Zaikovskii[c], and V. A. Likholobov[a]

[a] *Institute of Hydrocarbons Processing, Siberian Branch, Russian Academy of Sciences, Omsk, 644040 Russia*
[b] *Omsk State Technical University, Omsk, Russia*
[c] *Boreskov Institute of Catalysis, Siberian Branch, Russian Academy of Sciences, Novosibirsk, 630090 Russia*
e-mail: obelska@ihcp.oscsbras.ru

Received June 17, 2010

Abstract—A layered aluminum–magnesium hydroxide of the hydrotalcite type containing interlayer carbonate counterions (HT-CO_3) and activated hydrotalcite containing interlayer OH^- ions (HT-OH) were studied for the subsequent use as the precursors of supports for platinum catalysts. It was found that the nature of an interlayer anion in the composition of an aluminum–magnesium layered hydroxide is an important factor affecting both the formation of the oxide support and its texture characteristics. The replacement of the interlayer CO_3^{2-} anion by OH^- resulted in changes in the structural parameters of the initial double hydroxide: a decrease in the interlayer distance with the retention of the Mg/Al ratio and an increase in the imperfection of the layered material. X-ray diffraction studies in the temperature range of 30–900°C showed that HT-OH is characterized by the ability to form low-temperature spinel at 375°C. As a result, two types of aluminum–magnesium oxide supports, which were characterized by different pore space organizations at the same Mg : Al ratio, were obtained from the given layered hydroxides.

DOI: 10.1134/S0023158411050028

INTRODUCTION

Layered double hydroxides (LDHs) of the hydrotalcite type are widely used as the precursors of mixed aluminum–magnesium oxides. These latter are considered as potential substitutes for bases such as alkali metal hydroxides, ammonium salts, and amines [1], and they are used as the traps for NO_x [2], nickel, and vanadium [3]; they also catalyze the condensation and isomerization reactions of olefins, the alkylation of ketones and phenols, the selective reduction of unsaturated ketones and aldehydes, etc. [4–11].

Layered aluminum–magnesium hydroxides are obtained by the coprecipitation of Mg(II) and Al(III) cations in an alkaline medium [1–11] with a wide variation of a number of parameters affecting the purity, crystallinity, and particle size: pH, the concentration of reagents, the rate of their addition, and the temperature of aging [1]. The properties of LDHs as solid bases are determined by the presence of structural hydroxyl anions. However, the mixed oxides formed as a result of calcination exhibit strong Lewis basicity, which depends on not only the temperature of thermal treatment but also the nature of metals, the M^{2+}/M^{3+} ratio, and the properties of the interlayer anion in the layered hydroxide precursor [7–9]. The unique property of the mixed oxides to the restoration of a layered structure as a result of contact with water, a so-called memory effect, should be noted [9]. The layered structure formed by oxide reconstruction in water (activated hydrotalcite) exhibits catalytic activity because Brønsted OH^- groups appear as the compensating anions. It is important that the degree of reconstruction can be varied depending on the conditions of hydration [8]. Shiraga et al. [10] assumed that the most active and stable mixed oxide samples can be obtained with the use of the activated hydrotalcites.

At the same time, LDHs are attractive materials for preparing metal catalysts on basic supports, primarily, for selective hydrogenation processes [4–6, 10–13]. The majority of publications were related to the introduction of nickel, which is capable of isomorphously replacing a portion of magnesium in the brucite layers of a layered structure [14]. Note that, as a rule, the role of a supported metal is considered from the point of view of the modification of the properties of a hydroxide phase or a mixed oxide formed upon thermal treat-

ment. In this case, the influence of the nature of this type of carriers on the process of formation and the properties of metal centers of a bifunctional catalyst is not analyzed.

This series of publications is devoted to the synthesis and characterization of supported platinum catalysts obtained by the interaction of the chloride complexes of Pt(IV) with layered aluminum–magnesium hydroxides. The aim of this study was to use the layered structure of basic carriers for the formation of supported metal particles with unusual morphology and electronic and catalytic properties.

In this first communication, we report the results of a study of layered aluminum–magnesium hydroxides with different sizes and charges of counterions as the precursors of supports for platinum catalysts. For this purpose, we selected classical layered aluminum–magnesium hydroxide of the hydrotalcite type (HT-CO_3) and activated hydrotalcite (HT-OH), in the interlayer spaces of which the CO_3^{2-} and OH^- anions, respectively, were present. In this work, special attention is given to the role of the nature of a counterion and the structure of a hydroxide precursor in the process of the formation of an aluminum–magnesium oxide carrier and its texture characteristics. In the subsequent publications, we will report the results of a study of the interaction of platinum compounds with the test carriers and also data on the morphology and adsorption and catalytic properties of supported metal particles formed under straitened conditions of a layered structure. The catalytic properties of the resulting Pt/AlMgO_x supported systems will be tested in the model reactions of hydrocarbon conversion.

EXPERIMENTAL

Synthesis of the Support

The general approach to the synthesis of layered aluminum–magnesium hydroxides consists in the coprecipitation of Mg^{2+} and Al^{3+} from dilute solutions upon the addition of solutions containing carbonate and hydroxide ions to them [4, 5]. In this work, a solution of Mg(II) and Al(III) nitrates in a molar ratio of 3 : 1 was added drop by drop to a 1M solution of sodium carbonate, which was preheated to 60°C. In the course of coprecipitation, a constant value of pH 10 was adjusted by the addition of a solution of NaOH. After the addition of the entire volume of the solutions of nitrates, the suspension was stirred at 60°C for 1 h and then aged for 18 h at the same temperature. The resulting precipitate was filtered, washed with a large volume of water, and dried in air at 60°C for 12 h. This sample will be hereinafter referred to as HT-CO_3.

To prepare the HT-OH sample, the HT-CO_3 sample was calcined at 600°C and hydrated once again at $T = 25$°C for 24 h or at $T = 120$°C for 2 h. Both of the HT-CO_3 and HT-OH samples had the same molar ratio Mg : Al = 3.3 and contained 41.3 wt % magnesium and 13.7 wt % aluminum after calcination at 600°C. Metal concentrations in solutions after the dissolution of corresponding samples were determined by atomic absorption spectrometry with the use of an AA6300 SHIMADZU spectrometer.

Thermal analysis coupled with mass spectrometry (TA-MS). The TG-DTA method with mass spectrometry was used to study the thermal decomposition of hydrotalcite samples. The analysis of intermediate compounds and thermal decomposition products was carried out using an STA-449C Jupiter instrument (Netzsch) coupled to a QMS-403C Aeolos quadrupole mass spectrometer through a heated capillary. The measurements were performed in a dynamic mode in an atmosphere of argon. The rate of sample heating was 10 K/min. The sample weight was 10–20 mg.

High-resolution transmission electron microscopy (HRTEM). The HRTEM images were obtained on a JEM-2010 electron microscope (JEOL) with a lattice resolution of 0.14 nm at an accelerating voltage of 200 kV. Samples as suspensions in ethanol were applied to standard copper gauzes, which were introduced into the chamber of the electron microscope.

X-ray diffraction (XRD) analysis. XRD studies were performed on a D8 Advance diffractometer (Bruker) in parallel CuK_α radiation in the range of 2θ angles from 5 to 80°. The scanning step was 0.05°, and the signal integration time was 5 s/step.

The phase transformation dynamics of the layered aluminum–magnesium hydroxides was studied in an HTK 16 Anton Paar high-temperature chamber in the range of temperatures from 30 to 900°C. The step of a temperature change was 25 K over a temperature range of 25–400°C at a heating rate of 0.85 K/min. No considerable structural transformations were observed in the range of 400–900°C [15]; therefore, the step of a temperature change was increased to 100 K at a heating rate of 3.3 K/min. The interpretation of experimental data was accomplished with the use of the ICDD database. The structural characteristics were calculated with the use of the EVA and TOPAS program packages.

Low-temperature adsorption of nitrogen. The isotherms of nitrogen adsorption–desorption were measured at 77.4 K on an ASAP-2020 Micromeritics volumetric vacuum system. The range of equilibrium relative pressures was from 10^{-3} to 0.996 P/P_0. The BET specific surface areas (S_{BET}) were calculated from adsorption isotherms over the range of equilibrium relative values of $P/P_0 = 0.05$–0.25 for nitrogen vapor. In the calculation of specific surface areas, the molecular surface area of nitrogen in a filled monolayer was taken equal to 0.162 nm^2. The adsorption pore volume (V_{ads}) was determined from the adsorption of nitrogen at $P/P_0 = 0.990$ assuming that the adsorbate density was equal to the density of normal liquid (0.02887 mol/cm^3).

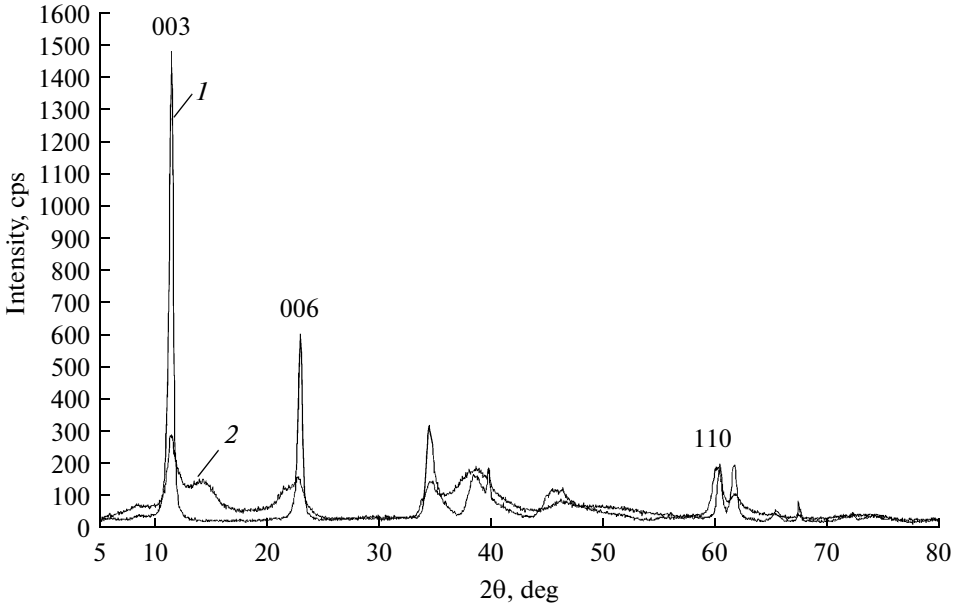

Fig. 1. Diffraction patterns of LDHs: (*1*) HT-CO_3 and (*2*) HT-OH.

The average pore diameter was evaluated according to the equation $D = 4V_{ads}/S_{BET}$. The BJH method for the desorption branches of isotherms was used to obtain differential characteristics—pore-size distribution curves (PSDCs). A cylindrical model of free pores was used in the calculations [16].

RESULTS AND DISCUSSION

XRD Analysis of LDHs and HR TEM Data

We compared the structural characteristics of the HT-CO_3 and HT-OH samples of layered aluminum–magnesium hydroxides. The results of their XRD analysis are analogous to those given in numerous publications [1–13]. The XRD patterns (Fig. 1) exhibit d_{003} and d_{110} basal reflections typical of these systems. The former characterizes the layered structure, and its position is affected by the size of the hydrated anion and the strength of the electrostatic interaction of hydroxide layers with the counteranion. The (110) peak position makes it possible to calculate the unit cell parameter a_0, which corresponds to the distance between two cations and reflects their radii. Furthermore, the parameter a_0 depends on the value of $x = Al/(Al + Mg)$, which determines the fraction of Al as a constituent of brucite-like layers, and decreases with x [17, 18].

At the same time, an analysis of the experimental diffraction patterns showed (Fig. 1, Table 1) that the replacement of the interlayer CO_3^{2-} anion by OH^- resulted in a decrease in the interplanar spacing d_{003} from 0.784 to 0.772 nm without noticeable changes in d_{110} (0.153 nm). In accordance with the current concepts of the structure of LDHs, a change in the interplanar spacing d_{003} can result from the joint action of two factors: the decrease of the size of the interlayer anion [18, 19] (it leads to a decrease in d_{003}) and the decrease of electrostatic interaction upon going from a double-charged ion to a singly charged ion (it leads to an increase in d_{003}). Differences were also observed in other structural characteristics: the lattice parameters a and c and the interlayer distance h, which was calculated as the difference between the interplanar spacing and the thickness of a brucite-like layer (0.48 nm) [18]. Similar values of the parameter d_{110} suggest that, in HT-OH prepared using the memory effect of calcined hydrotalcite, the same Mg : Al = 3 : 1 ratio as that in initial HT-CO_3 was retained.

Table 1. XRD data

Sample	d_{003}, Å	d_{110}, Å	$I(d_{003})$, cps	h, Å	FWHM, deg	CSR, Å	a, Å	c, Å
HT-CO_3	7.84	1.531	1484	3.04	0.39	240	3.064	23.544
HT-OH	7.72	1.534	288	2.92	0.86	110	3.075	23.177

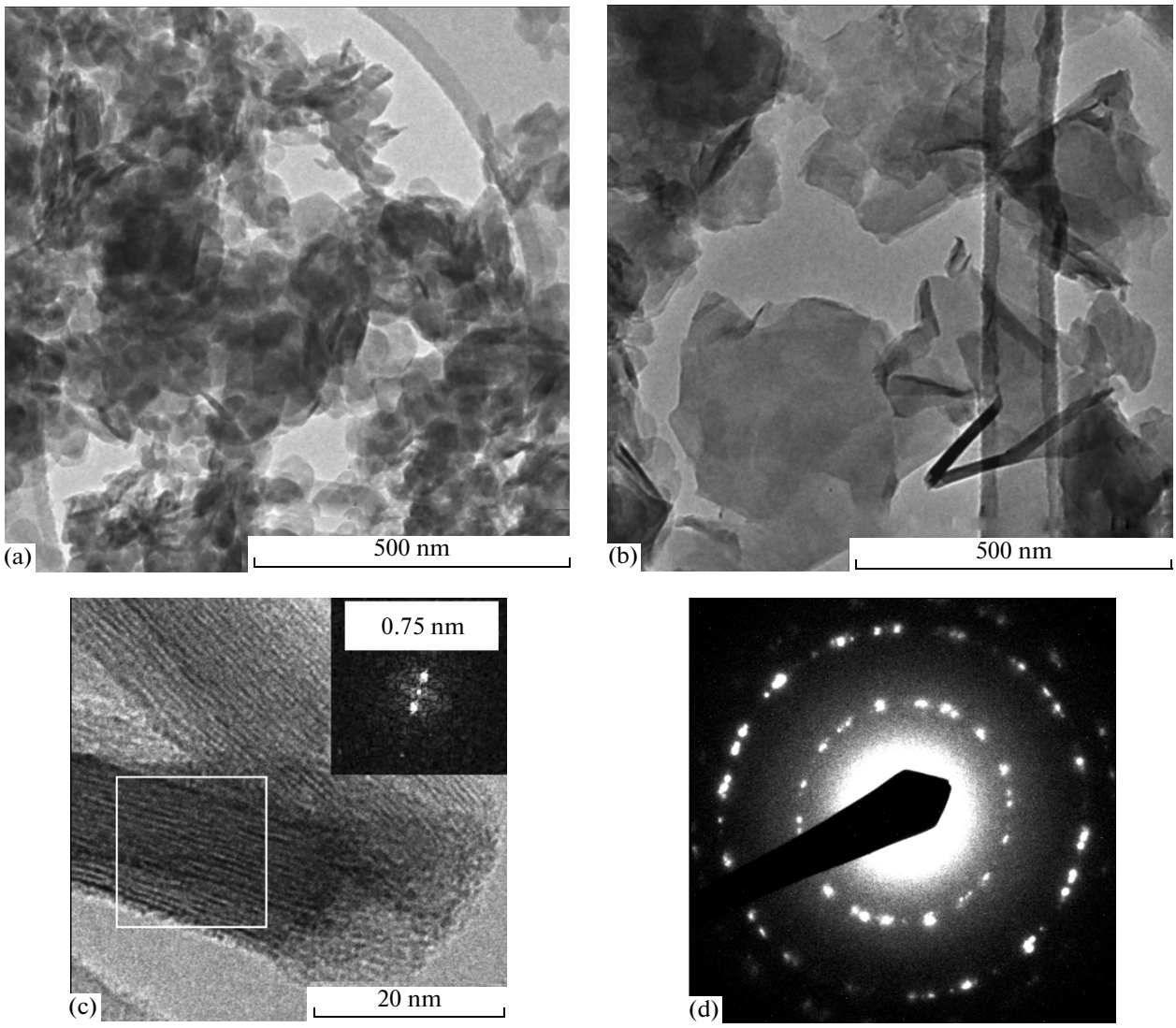

Fig. 2. Electron micrographs: particle morphology of (a) HT-CO_3 and (b) HT-OH samples; (c) layered structure of the HT-OH sample (insert: Fourier transform with the specified periodicity corresponding to hydrotalcite: $d_{003} \approx 0.75$ nm); and (d) electron microdiffraction, which represents the crystallographic texture for the plates of the HT-OH sample.

The observed broadening of peak profiles (FWHM) and, as a consequence, a decrease in the sizes of coherent scattering regions, as well as a significant decrease in the intensity of basal reflections upon the replacement of interlayer CO_3^{2-} anion by OH^- can result from a structural rearrangement, which manifested itself in an increase in the disorder of double hydroxide layers [18, 20].

Data on the XRD analysis of the HT-CO_3 and HT-OH aluminum–magnesium layered hydroxides agree well with the results of the TEM study of these samples. According to TEM data, the morphology of the particles of the HT-CO_3 and HT-OH samples was noticeably different. The particles of the HT-CO_3 sample (Fig. 2a) have a shape of thin rounded plates 10 to 20 nm in thickness with a width of 50–100 nm. In the HT-OH sample (Fig. 2b), the thickness of plates varied in a range from ~1 to 20 nm, and their width was much greater and reached 200–500 nm. In both samples, the particle structures were layered and formed by packets with a distance of about 0.75 nm between them (Fig. 2c), which is close to the interlayer spacing d_{003} of hydrotalcite. However, the structure of primary particles in the HT-OH sample was more defective. Probably, it was formed by microblocks in the form of parallel lamellas with sizes of 20 nm or greater. Their coalescence formed the secondary layered structure of the lamellar particles of the HT-OH sample with sizes up to 500 nm. The electron microdiffraction pattern (Fig. 2d) obtained in the direction of a normal to such plates with a microblock structure contains many reflections, which suggest the formation of a crystallo-

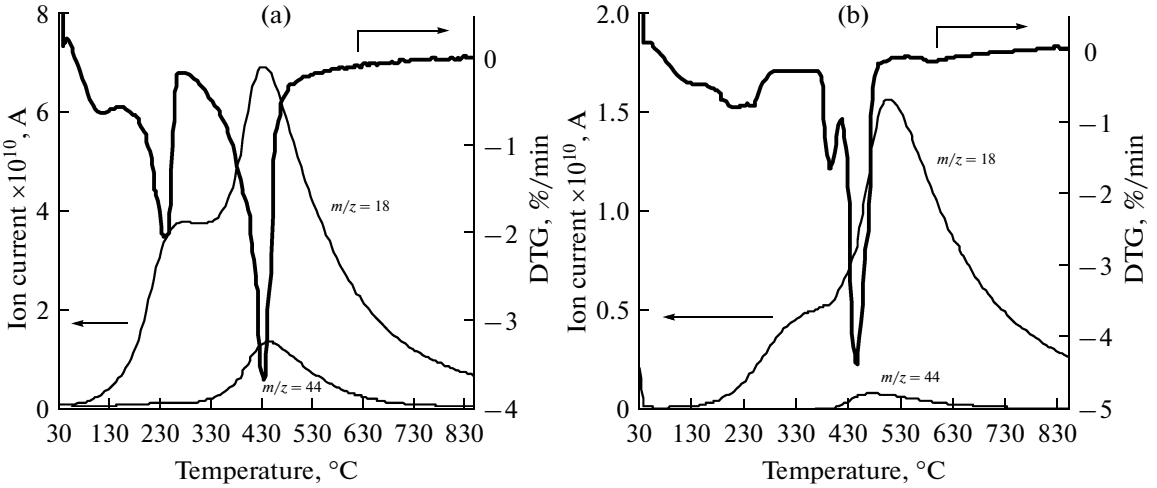

Fig. 3. DTG curves of (a) HT-CO_3 and (b) HT-OH LDH samples and the mass spectra of thermal decomposition products (H_2O, $m/z = 18$ and CO_2, $m/z = 44$).

graphic texture from the azimuthally disoriented layers.

Thermal Analysis of LDHs

Thermal analysis is one of the most important methods for investigating LDHs of the hydrotalcite type [6, 11]. The thermal behavior of the HT-CO_3 and HT-OH layered materials in the range of 30–900°C is characterized by two weight loss regions (Fig. 3) in close temperature ranges. According to published data [21–25], the loss of physically adsorbed and interlayer (structural) water occurs in the first region at temperatures lower than 300°C, and the dehydroxylation of hydroxide layers and the removal of charge-compensating anions occurs in the second region (300–500°C). This interpretation is consistent with the results of the mass-spectrometric analysis of the released products. Figure 3 shows the mass spectra for H_2O ($m/z = 18$) and CO_2 particles ($m/z = 44$) in the standard temperature–ion current strength coordinates.

The amount of structural water can be estimated as the difference between the weight loss in the first region (up to 300°C) and the weight loss at temperatures up to 100°C [13]. The presence of CO_2 in the thermal decomposition products of the HT-OH sample (in the region of 450°C) suggests the presence of an amount of carbonate counterions in the interlayer space of this sample. The simultaneous presence of two anions in the interlayer space was confirmed by the occurrence of two maximums in the profile of the (003) line [18] of the HT-OH sample (Fig. 1). The presence of carbonate counterions can result from the interaction of the carrier with dissolved carbon dioxide in the process of the hydration of aluminum–magnesium oxide.

An analysis of Fig. 3 showed that the observed difference in the total weight losses of the HT-CO_3 and HT-OH supports (43 and 33%, respectively) was mainly due to a noticeably smaller amount of structural water in the HT-OH sample. Furthermore, the thermogram of the HT-OH sample is characterized by two pronounced maximums in the temperature range of 350–500°C. The appearance of an additional DTG peak at 400°C can be explained by the formation of nonstoichiometric aluminum–magnesium spinel, which is confirmed by the results of thermal XRD studies given below.

Phase Transition Dynamics in the Temperature Range of 30–900°C

In this work, we studied the phase transition dynamics of the HT-CO_3 and HT-OH aluminum–magnesium layered hydroxides with different interlayer anions in the temperature chamber of a diffractometer over the temperature range of 30–900°C.

Figure 4 shows the data of the thermal XRD studies of the HT-CO_3 and HT-OH samples. From an analysis of the obtained diffraction patterns, it follows that a layered material with a hydrotalcite-like structure was retained in both of the samples at a temperature to 200°C, which corresponds to the removal of the main amount of interlayer structural water. Further heating leads to the formation of a so-called metaphase [18], which is stable in the temperature range of 200–375°C. The formation of this phase is characterized by a decrease in the interplanar spacing from 0.784 to 0.664 nm for HT-CO_3 or from 0.772 to 0.666 nm for HT-OH. As the temperature was increased above 400°C, the formation of a phase of MgO was observed in both of the samples. This is evidenced by the appearance of wide diffraction peaks with the 2θ val-

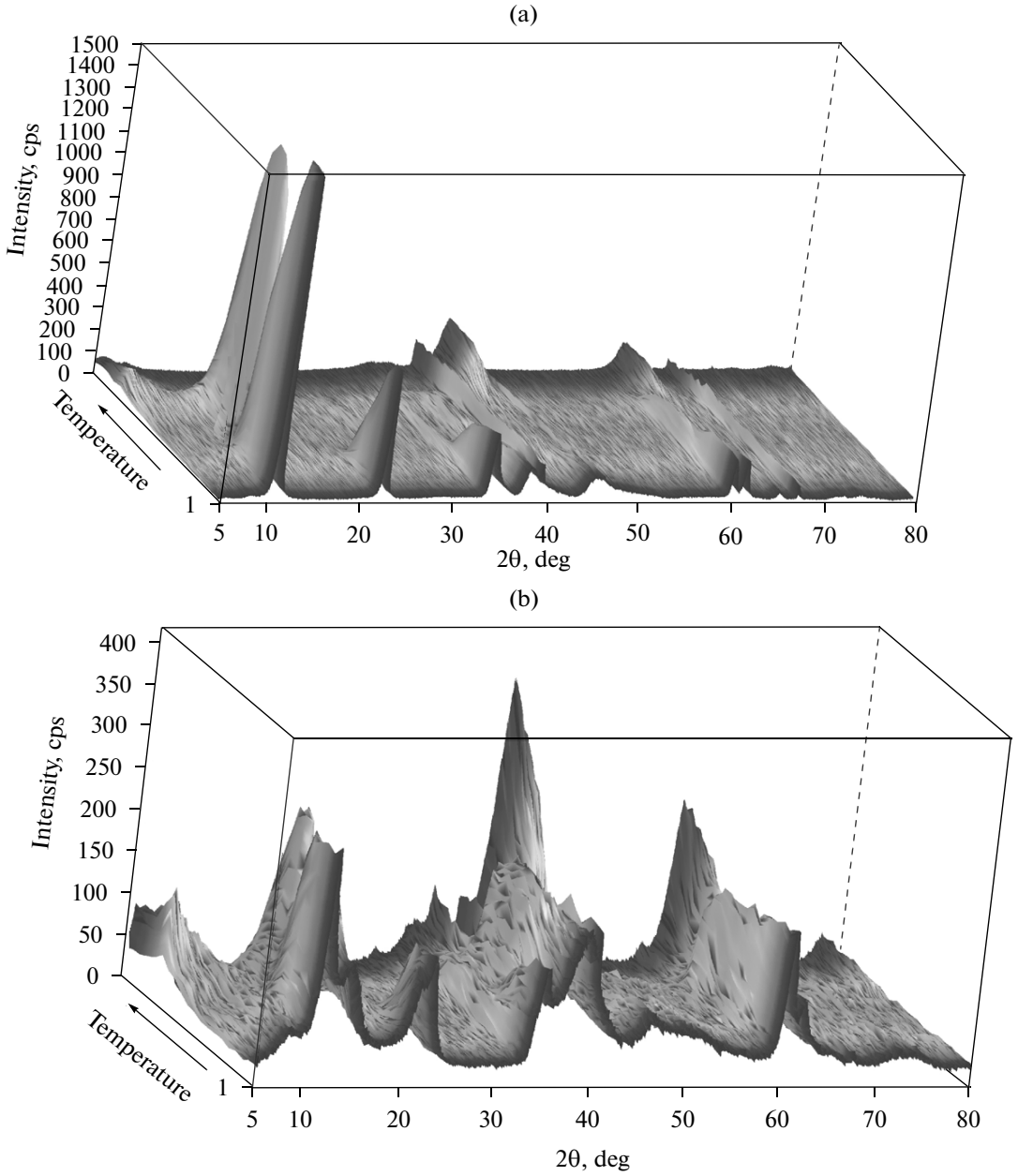

Fig. 4. Results of the thermal XRD analysis of (a) HT-CO_3 and (b) HT-OH LDH samples over the temperature range of 30–900°C.

ues of 42.91 and 62.28°. The unit cell parameter of the formed periclase-like structure was 0.4192 or 0.4208 nm for HT-CO_3 or HT-OH, respectively, as refined according to the least squares method. Furthermore, a halo, which is related to the presence of amorphous aluminum oxide [26], was observed in the diffraction patterns of both of the samples in the region of $2\theta = 35.5°$.

It is interesting that the formation of a fraction of the nonstoichiometric spinel $Mg_xAl_{1-x}O_4$ occurred only in the case of the HT-OH sample (Fig. 4b) starting at a temperature of 375°C; this spinel remained approximately constant up to 900°C. Usually, this phase was detected in a much higher temperature region (above 700°C) [25]. This manifested itself in the appearance of reflections at the 2θ values of 19.029, 31.272, 36.853, 44.833, 59.371, and 65.293 in the diffraction patterns.

The unit cell parameter of this spinel was determined in an individual experiment after heating the sample to 400°C in a chamber and keeping for 2 h at this temperature. It was 0.809 nm at the temperature of the experiment. The subsequent cooling led to a decrease in this parameter to 0.807 nm, which is

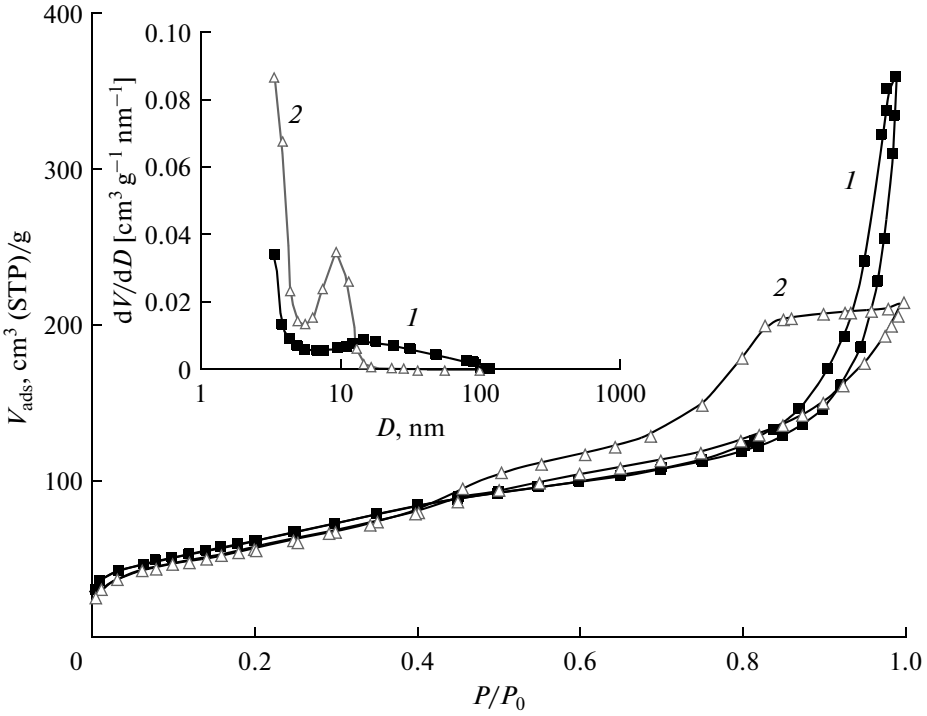

Fig. 5. Nitrogen adsorption–desorption isotherms for (*1*) HT-CO_3 and (*2*) HT-OH samples calcined at 600°C and (insert) pore-size distribution curves obtained from the desorption branch for the given samples.

somewhat smaller than the unit cell parameter of the stoichiometric spinel $MgAl_2O_4$, which is 0.808 nm [27].

Analysis of Texture Characteristics

We obtained the isotherms of nitrogen adsorption–desorption for the test samples; the shape of these isotherms corresponds to the type IV isotherms with a hysteresis loop characteristic of mesoporous materials (Fig. 5) [28].

The analysis of the texture characteristics of supports showed that the pore space and the surface are formed as a result of high-temperature treatment under the conditions that correspond to a change from a layered hydroxide phase to a mixed oxide phase. The thermal treatment of the HT-OH sample to 300°C did not lead to the development of its porosity; this is consistent with the absence of expressed processes from the thermogram in this temperature range (Fig. 3). Under the same thermal treatment conditions, the HT-CO_3 sample had a surface area of 59–67 m^2/g and a total pore volume of 0.275–0.361 cm^3/g (Table 2); the pores were formed as a result of the removal of weakly bound and interlayer water (Fig. 3). The calcination of the samples at 600°C resulted in the degradation of a layered structure, an increase in the specific surface areas of both samples to a level of 200 m^2/g, and an increase in the total pore volumes to 0.318 and 0.554 cm^3/g for the aluminum–magnesium oxides obtained from HT-OH and HT-CO_3, respectively.

The difference in the total pore volumes of the obtained mixed aluminum–magnesium oxides was due to the formation of their pore spaces in different pore size regions. The PSDC for the HT-CO_3 sample had a wide distribution with a diffuse maximum. In this case, the fraction of large pores (macro and meso) with diameters greater than 20 nm was higher than 60% of the total pore volume (Fig. 5, insert). The PSDC for the HT-OH sample exhibited a narrower distribution. The fraction of pores in the region of 5–16 nm with a maximum at 10 nm was about 65% of the total volume. The remainder of mesopores consisted of small pores with a diameter of <5 nm, and their fraction was greater than that in HT-CO_3 by a factor of 3. Note that large mesopores and macropores (a region of >20 nm), which are characteristic of the HT-CO_3 sample, were almost absent from the HT-OH sample.

Thus, the replacement of the interlayer CO_3^{2-} anion by OH^- in aluminum–magnesium layered hydroxides substantially influenced the process of texture formation in the oxide phase. In the resulting mixed oxides of the same chemical composition, the formation of a pore space occurs in different pore regions. The HT-CO_3 sample was formed as a macroporous material even at the stage of preparation, and the thermal treatment resulted only in an increase in the amount of pores without a change in their size. The HT-OH sample

Table 2. Main texture characteristics of the test samples according to nitrogen adsorption data (at 77 K)

Sample (calcination temperature)	S_{BET}, m^2/g	V_{ads}, cm^3/g	D, nm
HT-CO_3 (120°C)	59	0.288	19.6
HT-CO_3 (200°C)	61	0.275	18.1
HT-CO_3 (300°C)	67	0.361	21.6
HT-CO_3 (600°C)	229	0.554	9.7
HT-OH (120°C)	<1	0.001	–
HT-OH (200°C)	<1	0.016	–
HT-OH (300°C)	<1	0.013	–
HT-OH (600°C)	214	0.318	5.9

was nonporous at low temperatures, whereas the high-temperature treatment was accompanied by the formation of more uniform mesoporosity in the region to 20 nm.

CONCLUSIONS

The above studies showed that the HT-CO_3 and HT-OH LDHs, which have similar chemical composition of aluminum–magnesium layers (Mg/Al = 3) and formally differ only in the nature of interlayer anions, possess essentially different structure parameters. We found that the exchange of the interlayer CO_3^{2-} anion for the OH^- ions by the rehydration of the mixed aluminum–magnesium oxide through a memory effect leads to a decrease in the interplanar spacing d_{003} from 0.784 to 0.772 nm without noticeable changes in d_{110} (0.153 nm). Other structure characteristics also changed: lattice parameters a and c and interlayer distance h. The observed differences in the sizes of coherent scattering regions, the intensities of basal reflections, and the morphology of particles suggest a structural rearrangement, which leads to the disordering of double hydroxide layers of and an increase in the structure imperfection of the layered material.

As a result, differences in the process of formation of an oxide phase from the given hydroxide precursors are observed, and the resulting aluminum–magnesium oxide samples have different texture characteristics. Thus, we found for the first time that a phase of the low-temperature (375°C) nonstoichiometric spinel $Mg_xAl_{1-x}O_4$ is formed upon the thermal decomposition of HT-OH. We demonstrated the possibility (depending on the used LDH) of preparing both a predominantly coarsely porous oxide carrier (precursor, HT-CO_3) and a carrier with a predominant pore size smaller than 20 nm (predecessor, HT-OH) at close specific surface areas and the same chemical composition.

ACKNOWLEDGMENTS

We are grateful to T.P. Sorokina for providing us with a aluminum–magnesium LDH sample and to N.V. Antonicheva for performing the thermal analysis of the samples.

This work was supported by the Council of the President of the Russian Federation for Support of Young Scientists and Leading Scientific Schools (project no. NSh-5797.2008.3).

REFERENCES

1. Perez, C.N., Perez, C.A., Henriques, C.A., and Monteiro, J.L.F., *Appl. Catal., A*, 2004, vol. 272, p. 229.
2. Silletti, B.A., Adams, R.N., Sigmon, S.M., Nikolopoulos, A., Spivey, J.J., and Lamb, H.H., *Catal. Today*, 2006, vol. 114, p. 64.
3. Sorokina, T.P., Doronin, V.P., and Buluchevskaya, L.A., *Vserossiiskaya Tseolitnaya Konferentsiya "Tseolity i Mezoporistye Materialy: Dostizheniya i Perspektivy"* ("Zeolites and Mesoporous Materials: Achievements and Prospects," the Russian Conf. on Zeolites), Zvenigorod, Moscow oblast, 2008.
4. Cabello, F.M., Tichit, D., Coq, B., Vaccari, A., and Dung, N.T., *J. Catal.*, 1997, vol. 167, p. 142.
5. Tichit, D., Durand, R., Rolland, A., Coq, B., Lopez, J., and Marion, P., *J. Catal.*, 2002, vol. 211, p. 511.
6. Tsyganok, A.I., Inaba, M., Tsunoda, T., Suzuki, K., Takehira, K., and Hayakawa, T., *Appl. Catal., A,* 2004, vol. 275, p. 149.
7. Sels, B.F., de Vos, D.E., and Jacobs, P.A., *Catal. Rev.*, 2001, vol. 43, p. 443.
8. Abello, S., Dhir, S., Colet, G., and Perez-Ramirez, J., *Appl. Catal., A*, 2007, vol. 325, p. 121.

9. Liu, Y., Lotero, E., Goodwin, Jr.J.G., and Mo, X., *Appl. Catal., A*, 2007, vol. 331, p. 138.
10. Shiraga, M., Li, D., Atake, I., Shishido, T., Oumi, Y., Sano, T., and Takehira, K., *Appl. Catal., A*, 2007, vol. 318, p. 143.
11. Wu, G., Wang, X., Chen, B., Li, J., Zhao, N., Wei, W., and Sun, Y., *Appl. Catal., A*, 2007, vol. 329, p. 106.
12. Tichit, D., Lhouty, M.H., Guida, A., Chiche, B.H., Figueras, F., Aurous, A., Bartalini, D., and Garrone, E., *J. Catal.*, 1995, vol. 50.
13. Takehira, K., Shishido, T., Shouro, D., Murakami, K., Honda, M., and Takaki, K., *Appl. Catal., A*, 2005, vol. 279, p. 41.
14. Gerardin, C., Kostadinova, D., Sanson, N., Francova, D., Nanchoux, N., Tichit, D., and Coq, B., *Stud. Surf. Sci. Catal.*, 2005, vol. 156.
15. Kovanda, F., Rojka, T., Dobesova, J., Macovic, V., Bezdicka, P., Obalova, L., Jiratova, K., and Grygar, T., *J. Solid State Chem.*, 2006, vol. 179, p. 812.
16. Barrett, E.P., Joiner, L.G., and Halenda, P.H., *J. Am. Chem. Soc.*, 1951, vol. 73, p. 373.
17. Evance, D.G. and Slade, R.C.T., *Struct. Bond.*, 2006, vol. 119, p. 1.
18. Cavani, F., Trifiro, Fr., and Vacari, A., *Catal. Today*, 1991, vol. 11, p. 173.
19. Batsanov, S.S., *Strukturnaya khimiya: Fakty i zavisimosti* (Structural Chemistry: Facts and Relationships), Moscow: Dialog-MGU, 2000.
20. Umanskii, Ya.S., Skakov, Yu.A., Ivanov, A.M., and Rastorguev, L.I., *Kristallografiya, rentgenografiya i elektronnaya mikroskopiya* (Crystallography, X-ray Diffraction, and Electron Microscopy), Moscow: Metallurgiya, 1982.
21. Brindley, G.W. and Kikkawa, S., *Clays Clay Miner.*, 1980, vol. 28, p. 87.
22. Marino, O. and Mascolo, G., *Thermochim. Acta*, 1982, vol. 55, p. 377.
23. Roelofs, J., van Bokhoven, J.A., van Dillen, A.J., Geus, J.W., and de Jong, K.P., *Chem. Eur. J.*, 2002, vol. 8, p. 5571.
24. Yanga, W., Kima, Y., Liub, P.K.T., Sahimia, M., and Tsotsisa, T.T., *Chem. Eng. Sci.,* 2002, vol. 57, p. 2945.
25. Stanimirova, T., Vergilov, I., Kirov, G.., and Petrova, N., *J. Mater. Sci.*, 1999, vol. 34, p. 4153.
26. Brei, V.V., Melezhyk, O.V., Starukh, G.M., Oranskaya, E.I., and Mutovkin, P.A., *Microporous Mesoporous Mater.*, 2008, vol. 113, p. 411.
27. Pattern 21-1152, ICDD, PDF-2, 2006.
28. Sing, K.S.W., Everett, D.H., and Haul, R.A.W., *Pure Appl. Chem.*, 1985, vol. 57, no. 4, p. 603.